

Electronic Supplementary Material (ESI) for Journal of Materials Chemistry C.

Electronic Supplementary Information

Intramolecular H-bond Design for Efficient Orange-Red Thermally Activated Delayed Fluorescence Based on Rigid Dibenzo[f,h]pyrido[2,3-b]quinoxaline Acceptor

Feng-Ming Xie,¹ Xin-Yi Zeng,¹ Jing-Xiong Zhou,¹ Zhi-Dong An,¹ Wenjun Wang,³
Yan-Qing Li,^{1,2,*} Xiao-Hong Zhang,¹ Jian-Xin Tang^{1,*}

¹ *Jiangsu Key Laboratory for Carbon-Based Functional Materials & Devices, Institute
of Functional Nano & Soft Materials (FUNSOM), Soochow University, Suzhou,
Jiangsu 215123, China*

² *School of Physics and Electronics Science, Ministry of Education Nanophotonics &
Advanced Instrument Engineering Research Center, East China Normal University,
Shanghai, 200062, China*

³ *School of Physical Science and Information Technology, Shandong Provincial Key
Laboratory of Optical Communication Science and Technology, Liaocheng
University, Shandong 252059, China*

* Corresponding authors. E-mail: yqli@phy.ecnu.edu.cn (Y.-Q. Li),
jxtang@suda.edu.cn (J.-X. Tang)

Experimental Section

Chemical Synthesis: All the reagents were purchased from commercial sources and used without further purification. All the reactions were performed under nitrogen atmosphere, and the crude products were purified by column chromatography before material characterizations and device fabrication.

Materials Characterization: Chemical structures were determined by ^1H and ^{13}C nuclear magnetic resonance (NMR) spectra with a Bruker AVANCE III type NMR Spectrometer in CDCl_3 solution, and ultrafleXtreme MALDI-TOF mass spectrometer. Ultraviolet-visible absorption and photoluminescence (PL) spectra were recorded at room temperature with a Perkin-Elmer Lambda 750 UV-Vis spectrophotometer and a FM-4 type fluorescence spectrophotometer (JY company, French), respectively. Optical bandgap (E_g) was determined from the onset of the absorption spectra. Low-temperature fluorescence and phosphorescence spectra were measured with a FLS 920 spectrometer (Einburgh Corporation) in toluene at 77 K. Absolute photoluminescence quantum yields (PLQYs) of neat and doped films thermally deposited on quartz substrates were obtained with a C9920-02G type fluorescence spectrophotometer (HAMAMASTU, Japan) with an integrating sphere at room temperature under nitrogen atmosphere. Transient PL decay curves of the films were measured with a Quantaaurus-Tau fluorescence lifetime spectrometer (C11367-32, Hamamatsu Photonics) with an excitation wavelength of 373 nm under vacuum atmosphere. Low-temperature measurements were conducted using a cryostat (Oxford Optistat DN). Cyclic voltammetry (CV) measurements were conducted on a RST 3100 electrochemical work

station. Thermal gravimetric analysis (TGA) was conducted with a HCT-2 instrument. Differential scanning calorimetry (DSC) was performed on a Pyris Diamond DSC thermal analyzer.

Theoretical Calculations: All the quantum chemical calculations were performed using a DFT method in Gaussian 09 program package. The ground-state geometries were optimized by using a TD-DFT approach at the B3LYP/6-31G(d) level. The singlet and triplet excited-state properties were calculated according to the optimized geometries.

Device Fabrication and Measurements: OLEDs were fabricated on the patterned indium-tin-oxide (ITO)-coated glass substrates with a sheet resistance of $\sim 15 \Omega$ per square. The ITO-coated glass substrates were successively cleaned in ultrasonic baths with acetone, ethanol, and deionized water, and then dried in an oven at $110 \text{ }^\circ\text{C}$. The ITO-coated glass substrates were transferred into a high-vacuum deposition chamber (base pressure $\leq 2 \times 10^{-6}$ mbar) for the thermal deposition of organic materials and metal electrodes through shadow masks. Layer thickness and deposition rate were monitored by an oscillating quartz thickness monitor. The active area of OLEDs was defined to be 10 mm^2 . The fabricated devices were transferred to an interconnected nitrogen-filled glovebox for the encapsulation with a glass cap and epoxy glue. Current density-voltage-luminance (J-V-L) characteristics and EL spectra of the devices were measured simultaneously with a source meter (Keithley model 2400) and a luminance meter/spectrometer (PhotoResearch PR670). The CIE 1931 color coordinates were obtained from the EL spectra. The EQE values were calculated by assuming an ideal Lambertian emission profile, which were verified by the independent measurements of

luminous flux with an integrating sphere (Hamamatsu Photonics K.K. C9920-12).

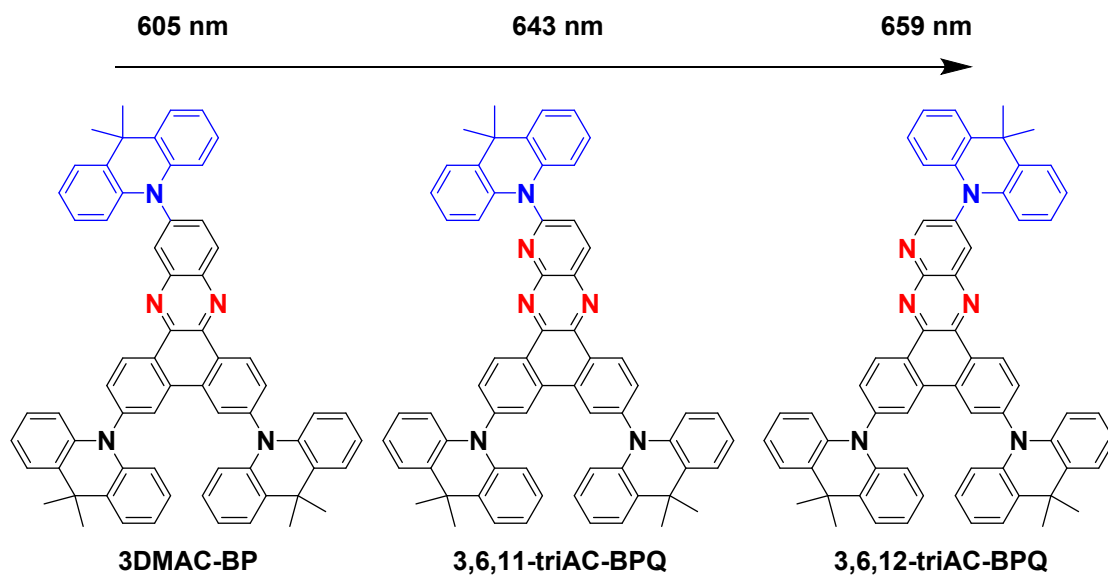


Figure S1. Molecular structures of 3DMAC-BP, 3,6,11-triAC-BPQ and 3,6,12-triAC-BPQ as well as emission peak in neat films.

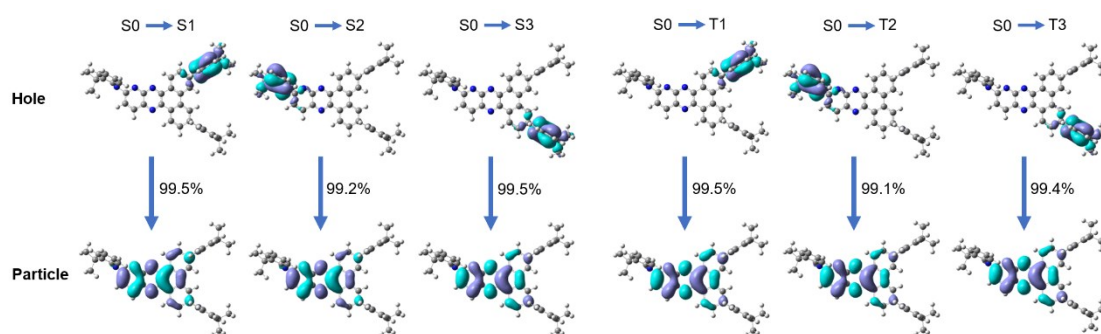


Figure S2. Natural transition orbital (NTO) analysis for 3,6,11-triAC-BPQ.

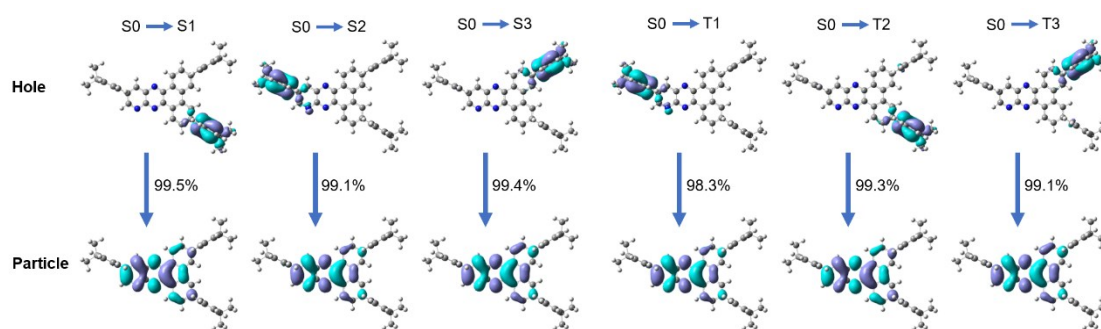


Figure S3. Natural transition orbital (NTO) analysis for 3,6,12-triAC-BPQ.

Table S1. Crystal data and structure refinement for 3,6,11-triAC-BPQ.

CCDC	2024221
Empirical formula	C ₆₄ H ₅₀ N ₆
Formula weight	903.10
Temperature/K	140.0
Crystal system	monoclinic
Space group	C2/c
a/Å	19.5271(11)
b/Å	14.5786(8)
c/Å	40.638(2)
α /°	90
β /°	95.065(2)
γ /°	90
Volume/Å ³	11523.5(11)
Z	8
ρ calc/cm ³	1.041
μ /mm ⁻¹	0.061
F(000)	3808.0
Crystal size/mm ³	0.15 × 0.08 × 0.05
Radiation	MoK α (λ = 0.71073)
2 Θ range for data collection/°	3.936 to 50.144
Index ranges	-23 ≤ h ≤ 23, -17 ≤ k ≤ 17, -48 ≤ l ≤ 45
Reflections collected	45785
Independent reflections	10005 [R _{int} = 0.0623, R _{sigma} = 0.0596]
Data/restraints/parameters	10005/0/637
Goodness-of-fit on F ²	1.029
Final R indexes [$I \geq 2\sigma(I)$]	R ₁ = 0.0548, wR ₂ = 0.1343
Final R indexes [all data]	R ₁ = 0.0823, wR ₂ = 0.1471
Largest diff. peak/hole / e Å ⁻³	0.20/-0.27

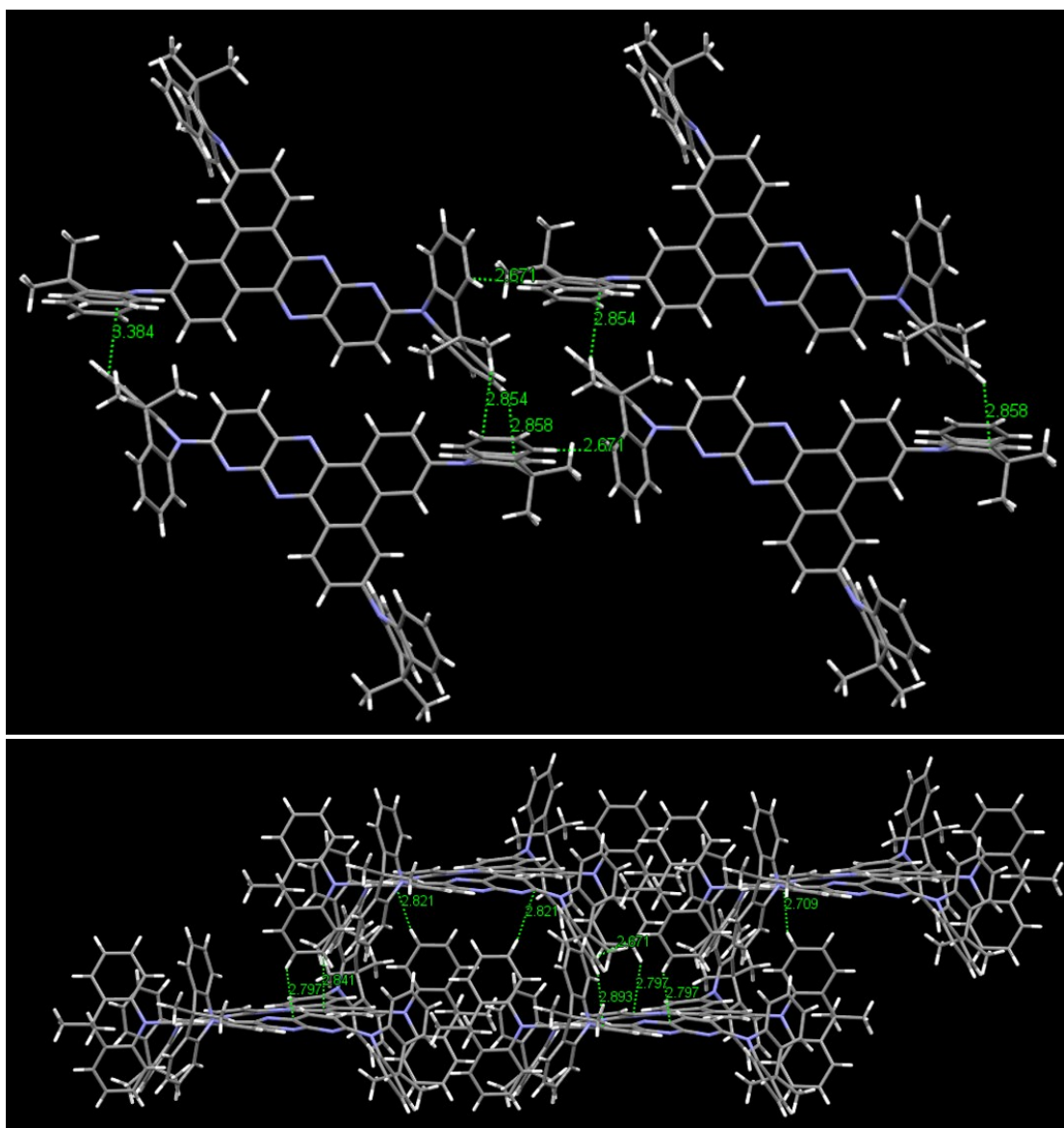


Figure S4. Molecular packing of 3,6,11-triAC-BPQ.

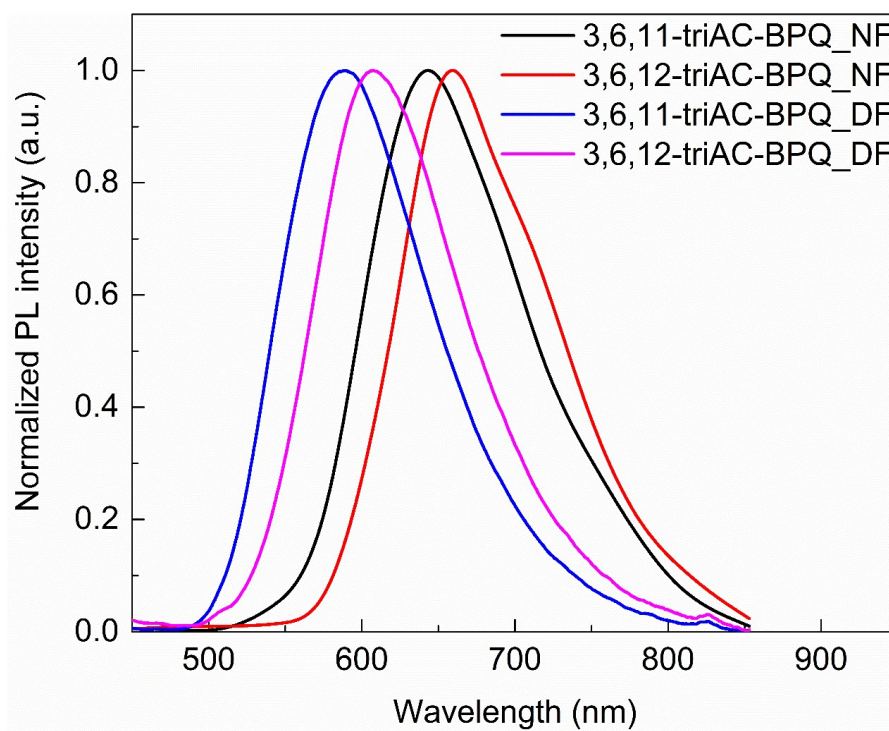


Figure S5. PL spectra of 3,6,11-triAC-BPQ and 3,6,12-triAC-BPQ in neat film (NF), and doped film (DF).

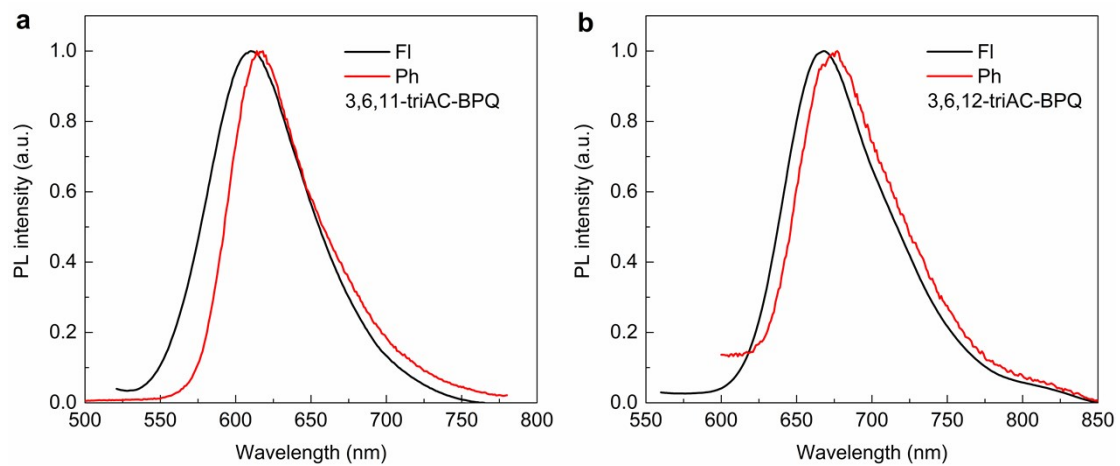


Figure S6. Low-temperature fluorescence spectra and phosphorescence spectra of (a) 3,6,11-triAC-BPQ and (b) 3,6,12-triAC-BPQ were measured in neat film at 77 K.

$S_1=2.27/2.02$ eV, $T_1= 2.17/1.99$ eV, $\Delta E_{S1}=0.10/0.03$ eV, respectively.

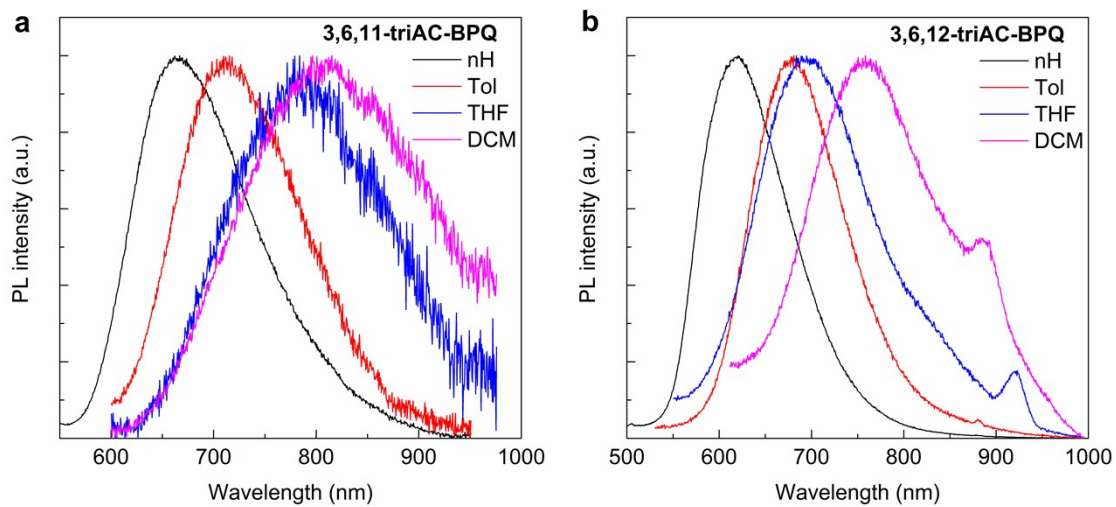


Figure S7. PL spectra of 3,6,11-triAC-BPQ and 3,6,12-triAC-BPQ in various solvents.

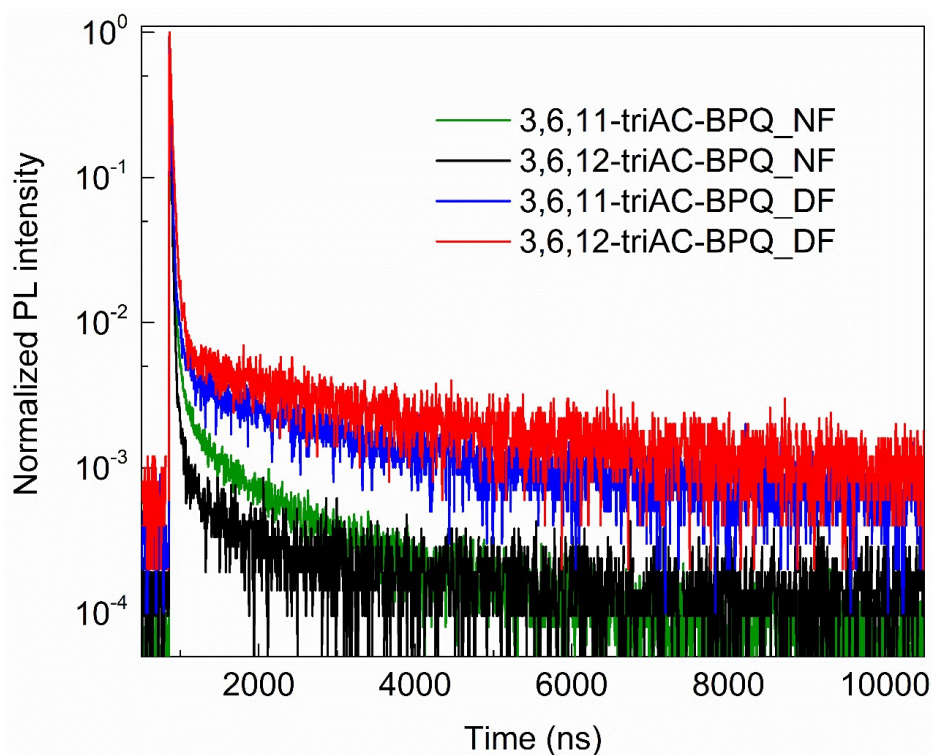


Figure S8. Transient PL decays of 3,6,11-triAC-BPQ and 3,6,12-triAC-BPQ in neat films (NF), and doped films (DF).

Table S2. Photophysical characteristics of 3,6,11-triAC-BPQ and 3,6,12-triAC-BPQ.

Dopants	Φ_p	Φ_d	τ_p	τ_d	k_{PF}	k_{DF}	k_r	k_{nr}	k_{ISC}	k_{RISC}	k_{TADF}
	[%]	[%]	[ns]	[μ s]	[10^7 s $^{-1}$]	[10^5 s $^{-1}$]	[10^7 s $^{-1}$]	[10^7 s $^{-1}$]	[10^7 s $^{-1}$]	[10^5 s $^{-1}$]	[10^5 s $^{-1}$]
3,6,11- triAC-BPQ	42.5	32.5	11.9	2.50	8.40	4.00	3.59	1.19	3.62	7.09	1.3
3,6,12- triAC-BPQ	20	33	15.4	2.25	6.49	4.44	1.19	1.15	4.05	12.01	1.47

¹ Radiative rate constants of S₁, $k_r = \Phi_p/\tau_p + \Phi_d/\tau_d$.

² Nonradiative rate constants of S₁, $k_{nr} = k_r(1 - \Phi_{PL})/\Phi_{PL}$.

³ Rate constants for ISC (S₁ → T₁), $k_{ISC} = k_p - k_r - k_{nr}$.

⁴ Rate constants for RISC (T₁ → S₁), $k_{RISC} = k_p k_d / k_{ISC} \cdot \Phi_d / \Phi_p$.

⁵ Rate constants for TADF, $k_{TADF} = \Phi_d / \tau_d$.

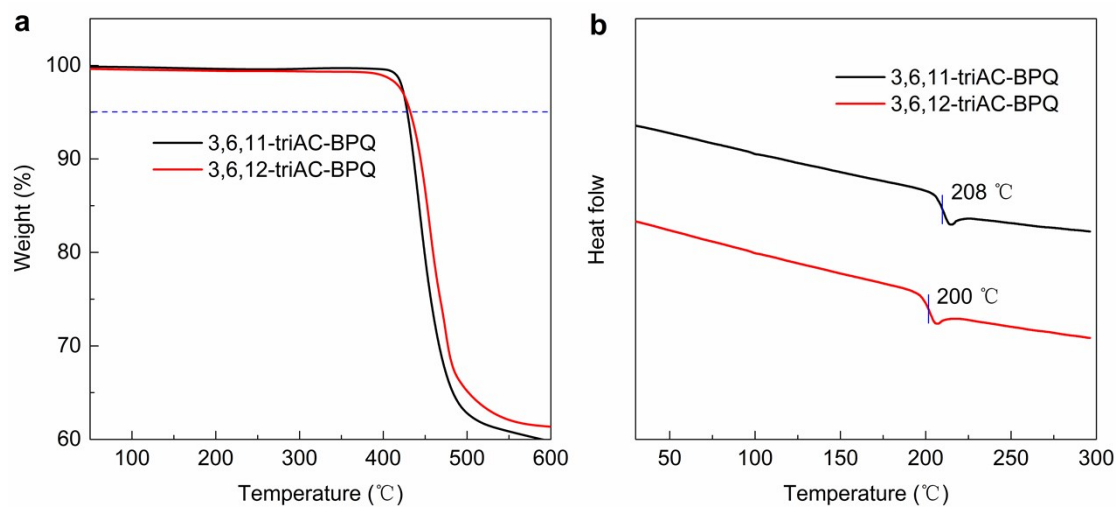


Figure S9. a) Thermogravimetric analysis (TGA) and b) differential scanning calorimetry (DSC) curves.

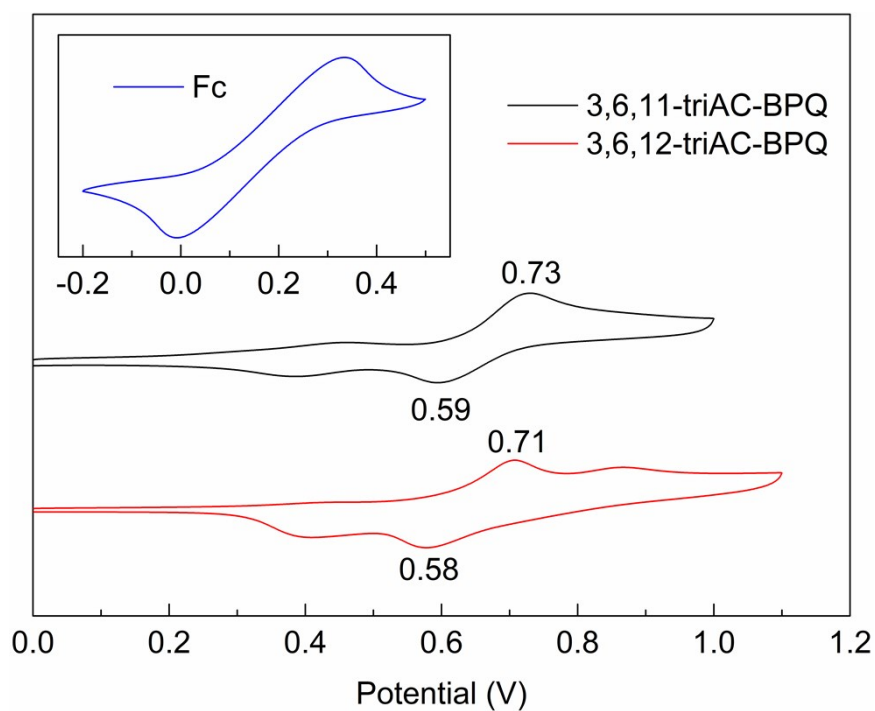


Figure S10. Cyclic voltammetry (CV) curves.

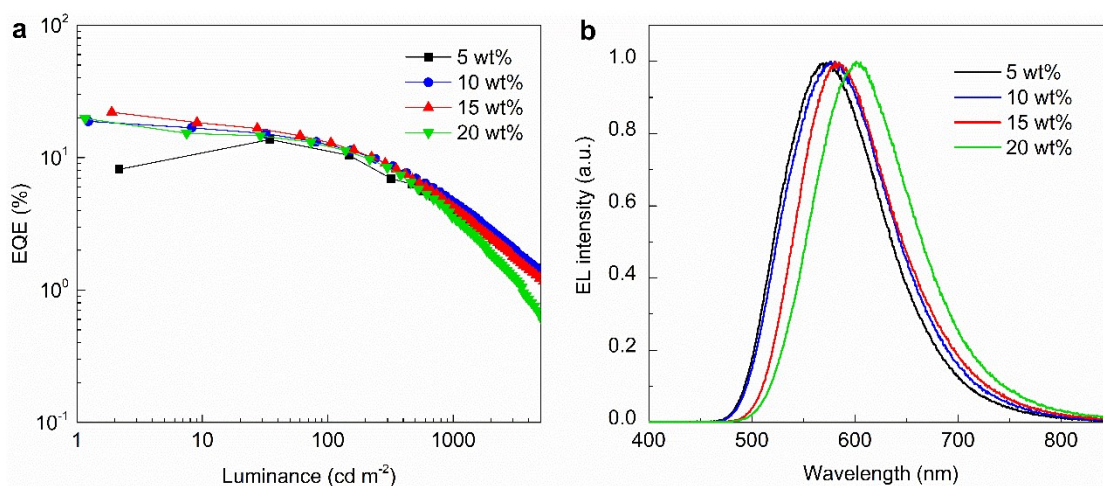


Figure S11. Device performance of OLEDs based on 3,6,11-triAC-BPQ with different doping concentrations. a) EQE as a function of luminance. b) EL spectra.

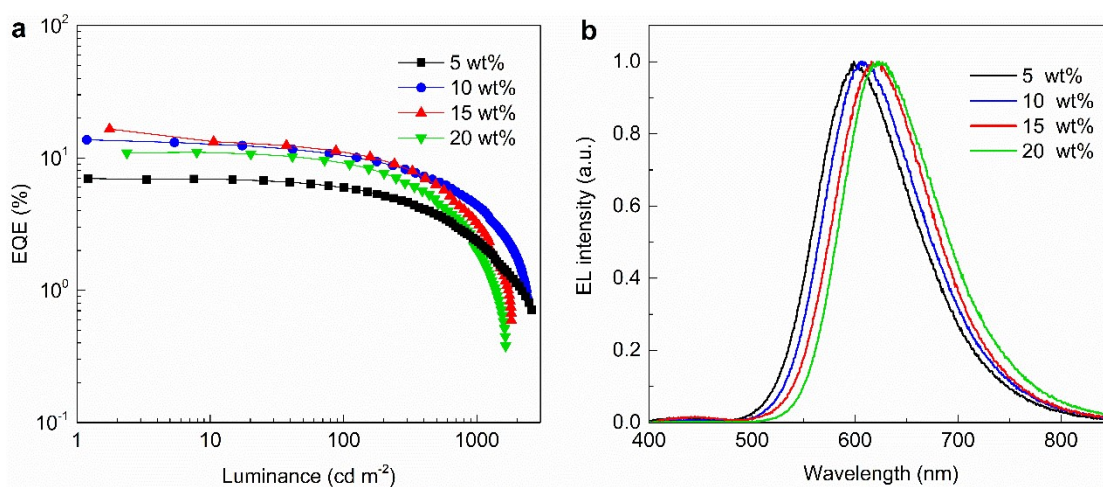
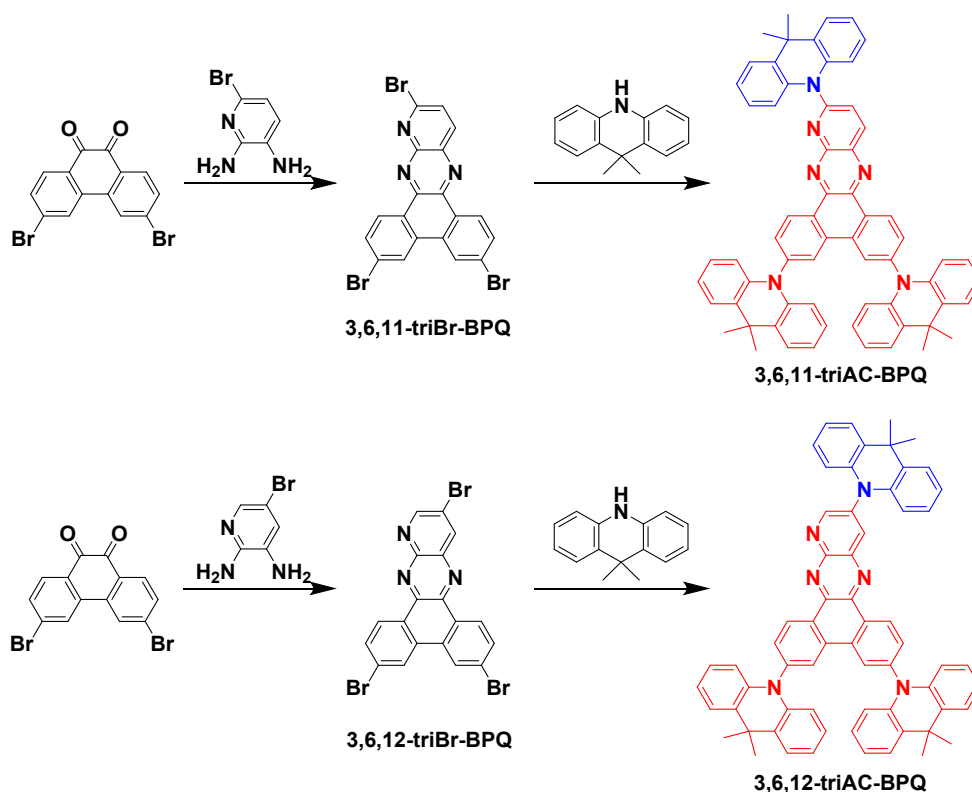


Figure S12. Device performance of OLEDs based on 3,6,12-triAC-BPQ with different doping concentrations. a) EQE as a function of luminance. b) EL spectra.



Scheme S1. Synthetic routes of 3,6,11-triAC-BPQ and 3,6,12-triAC-BPQ.

3,6,11-tribromodibenzo[f,h]pyrido[2,3-b]quinoxaline (3,6,11-triBr-BPQ)

3,6-dibromophenanthrene-9,10-dione (0.50 g, 1.36 mmol) and 6-bromopyridine-2,3-diamine (0.28 g, 1.49 mmol) were added into 100 mL ethanol. The mixture solution was refluxed at 90 °C under N₂ atmosphere. The precipitate was collected by filtration and washed with sufficient ethanol to obtain the purified 3,6,11-triBr-BPQ for the next reaction. Yield: 0.62 g (88%).

3,6,11-tris(9,9-dimethylacridin-10-yl)dibenzo[f,h]pyrido[2,3-b]quinoxaline (3,6,11-triAC-BPQ)

3,6,11-triBr-BPQ (0.32 g, 0.618 mmol), 9,9-dimethylacridan (0.40 g, 1.91 mmol) and *t*-BuONa (0.40 g, 4.16 mmol) were dissolved in 40 mL toluene. Then, Pd₂(dba)₃ (5% equi) and *t*-Bu₃PHBF₄ (5% equi) were added in a nitrogen atmosphere. After the

solution was heated at 110 °C for 24 hours, the reaction mixture was cooled to room temperature. The product was extracted with DCM. The crude product was further purified by silica gel column chromatography (DCM : PE = 1 : 3) to give 0.45 g (yield: 80%) of **3,6,11-triAC-BPQ** as an orange-red powder. ¹H NMR (400 MHz, CDCl₃) δ 9.82 (d, *J* = 8.5 Hz, 1H), 9.61 (d, *J* = 8.5 Hz, 1H), 8.45-8.36 (m, 3H), 8.25 (d, *J* = 8.0 Hz, 2H), 7.87 (d, *J* = 9.4 Hz, 1H), 7.74 (ddd, *J* = 13.4, 8.6, 1.7 Hz, 2H), 7.55 (d, *J* = 7.8 Hz, 2H), 7.50-7.41 (m, 6H), 7.32 (t, *J* = 7.6 Hz, 2H), 6.95-6.86 (m, 8H), 6.36-6.28 (m, 4H), 1.69 (d, *J* = 23.5 Hz, 18H). ¹³C NMR (101 MHz, CDCl₃) δ 157.21, 150.38, 143.94, 143.58, 142.77, 142.33, 140.72, 140.68, 139.87, 139.73, 138.92, 136.08, 134.38, 133.40, 131.55, 131.39, 130.40, 130.10, 130.06, 130.00, 129.95, 128.75, 126.47, 126.35, 126.01, 125.83, 125.53, 125.39, 123.84, 120.77, 118.38, 114.07, 38.14, 36.01, 31.74, 31.70, 26.79. MALDI-TOF MS (ESI, *m/z*) calcd for C₆₄H₅₀N₆ [M⁺]: 902.41, Found: 903.339.

3,6,12-tris(9,9-dimethylacridin-10-yl)dibenzo[f,h]pyrido[2,3-b]quinoxaline

(3,6,12-triAC-BPQ)

3,6,12-triAC-BPQ was prepared by the same procedure with **3,6,11-triAC-BPQ** excepting using the 5-bromopyridine-2,3-diamine (0.28 g, 1.49 mmol), leading to a red solid of **3,6,12-triAC-BPQ** (0.43 g, yield: 77%). ¹H NMR (400 MHz, CDCl₃) δ 9.89 (d, *J* = 8.5 Hz, 1H), 9.67 (d, *J* = 8.5 Hz, 1H), 9.33 (d, *J* = 2.5 Hz, 1H), 8.86 (d, *J* = 2.5 Hz, 1H), 8.47 (s, 2H), 7.81 (dd, *J* = 17.2, 8.5 Hz, 2H), 7.58 (dd, *J* = 5.9, 3.3 Hz, 2H), 7.51-7.43 (m, 4H), 7.09 (p, *J* = 6.8 Hz, 4H), 7.00-6.88 (m, 8H), 6.64-6.57 (m, 2H), 6.39-

6.28 (m, 4H), 1.81-1.69 (m, 18H). ^{13}C NMR (101 MHz, CDCl_3) δ 157.95, 148.80, 144.66, 144.58, 144.49, 143.54, 140.56, 140.33, 139.08, 138.31, 137.93, 134.74, 132.23, 132.03, 130.43, 130.25, 130.21, 129.73, 129.58, 129.30, 126.74, 126.49, 126.30, 126.16, 125.63, 125.59, 122.34, 120.97, 115.22, 114.13, 114.05, 36.40, 36.04, 31.65, 31.63, 30.68. MALDI-TOF MS (ESI, m/z) calcd for $\text{C}_{64}\text{H}_{50}\text{N}_6$ [M^+]: 902.41, Found: 903.368.

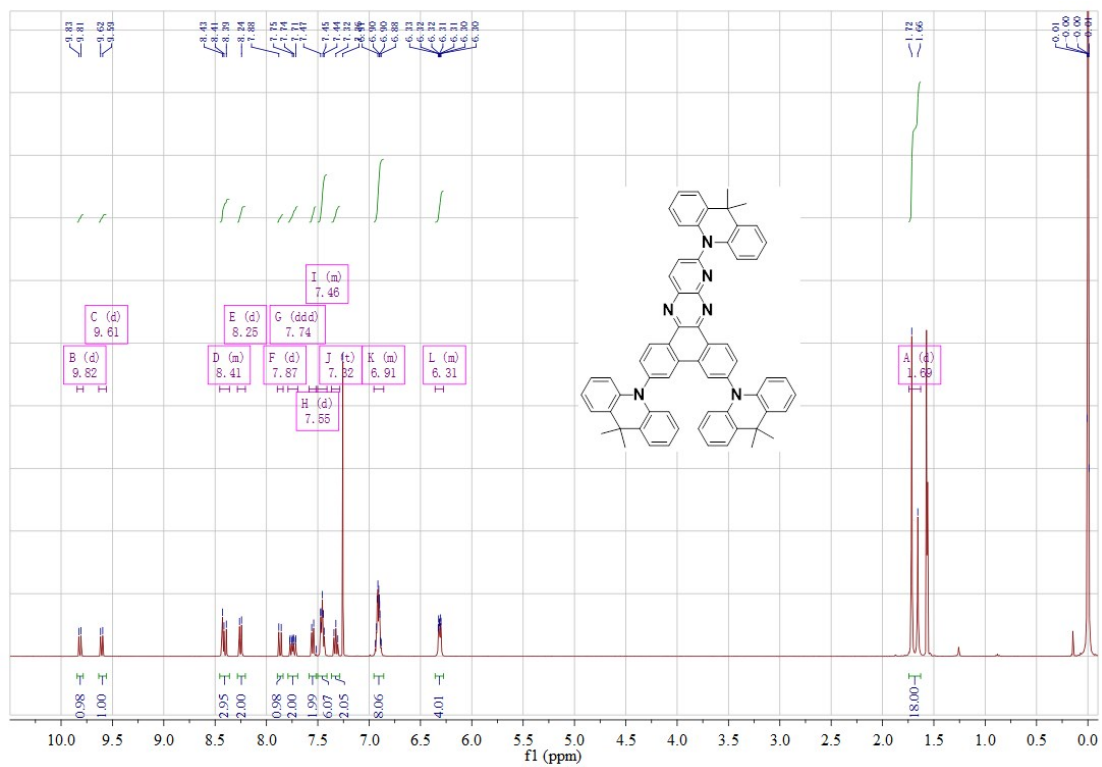


Figure S13. ^1H NMR spectra of 3,6,11-triAC-BPQ.

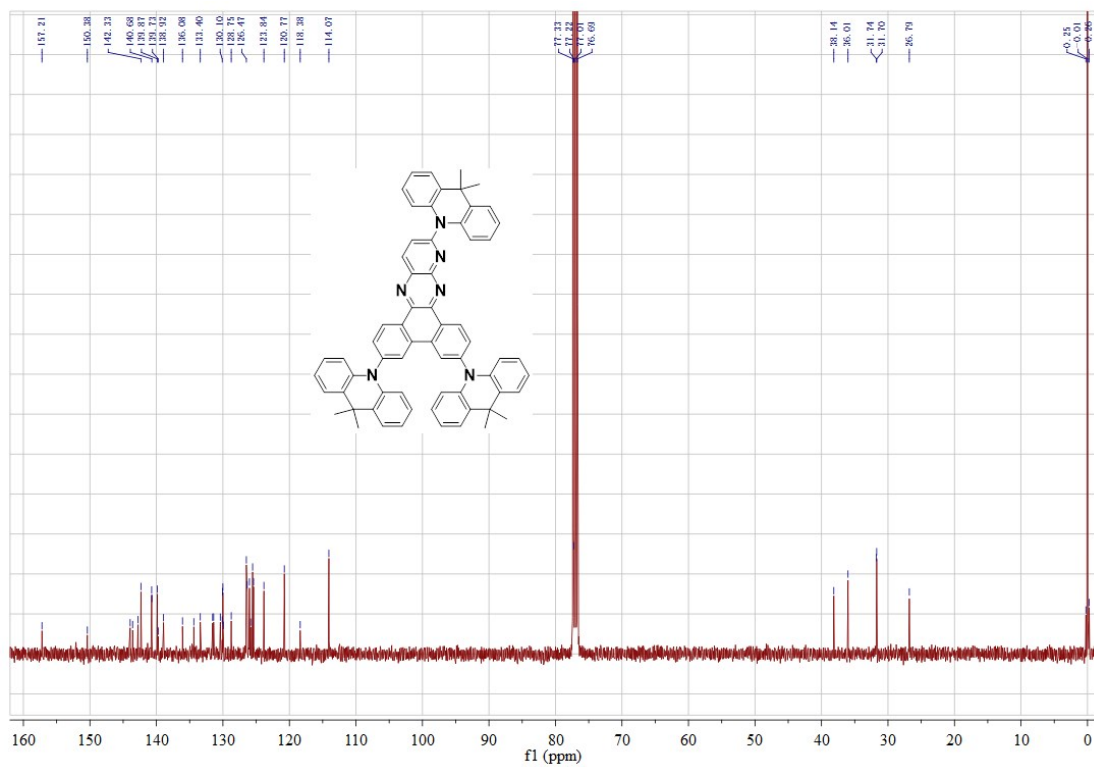


Figure S14. ^{13}C NMR spectra of 3,6,11-triAC-BPQ.

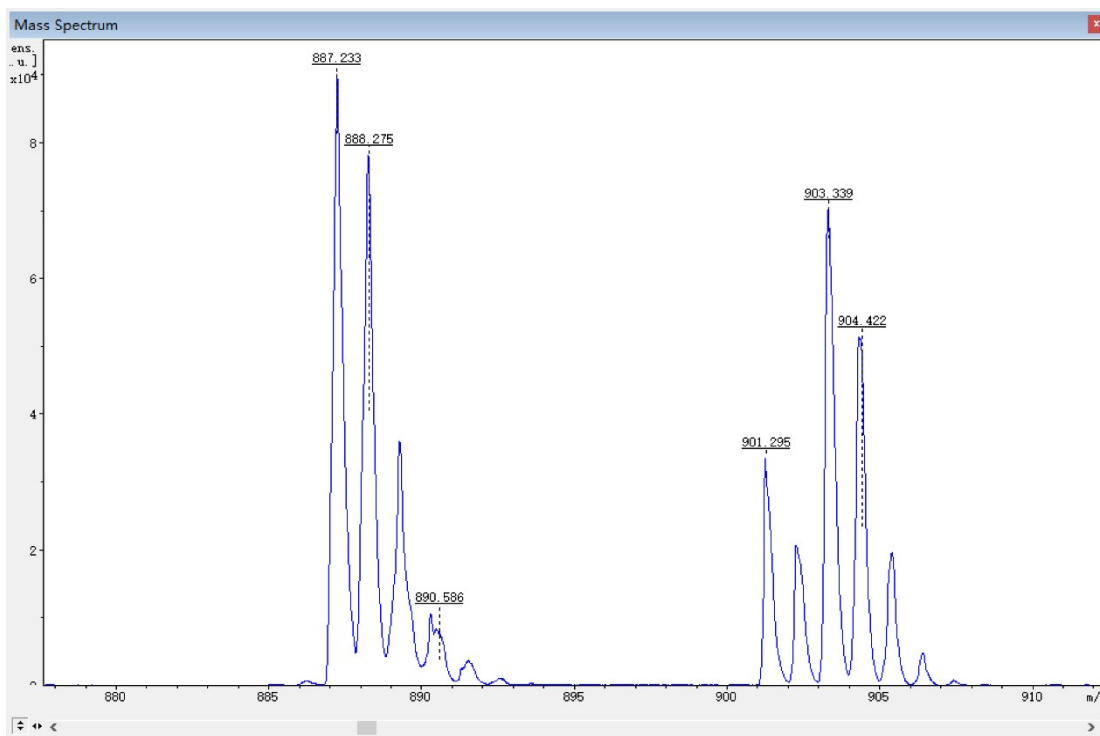


Figure S15. MALDI-TOF MS spectra of 3,6,11-triAC-BPQ.

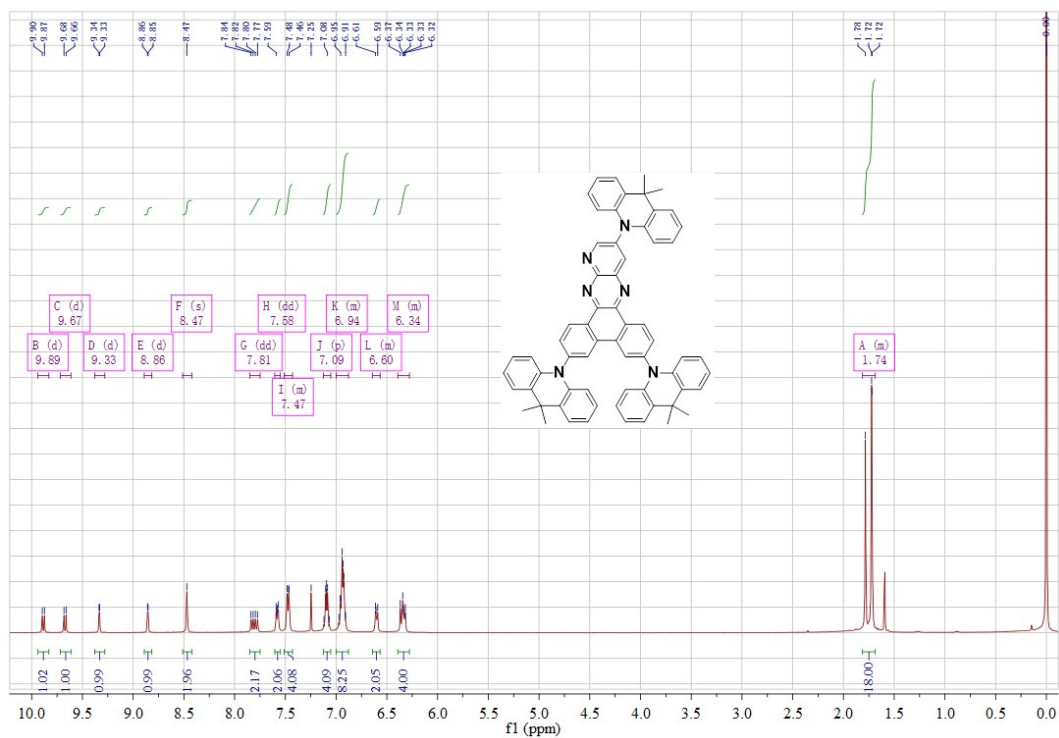


Figure S16. ^1H NMR spectra of 3,6,12-triAC-BPQ.

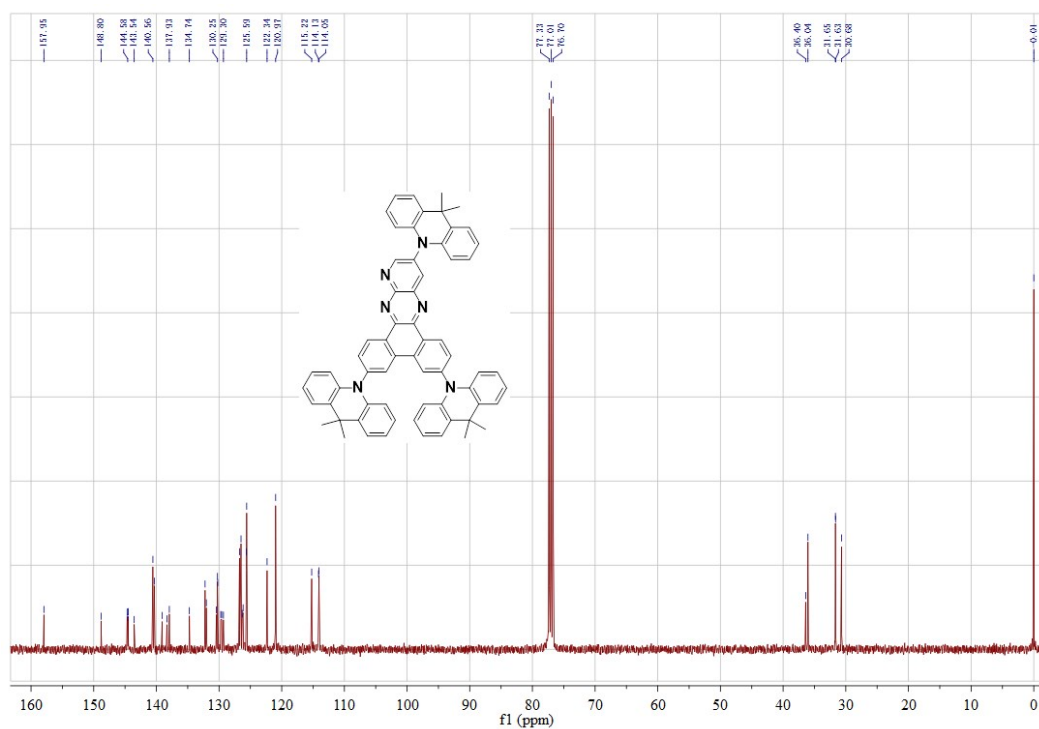


Figure S17. ^{13}C NMR spectra of 3,6,12-triAC-BPQ.

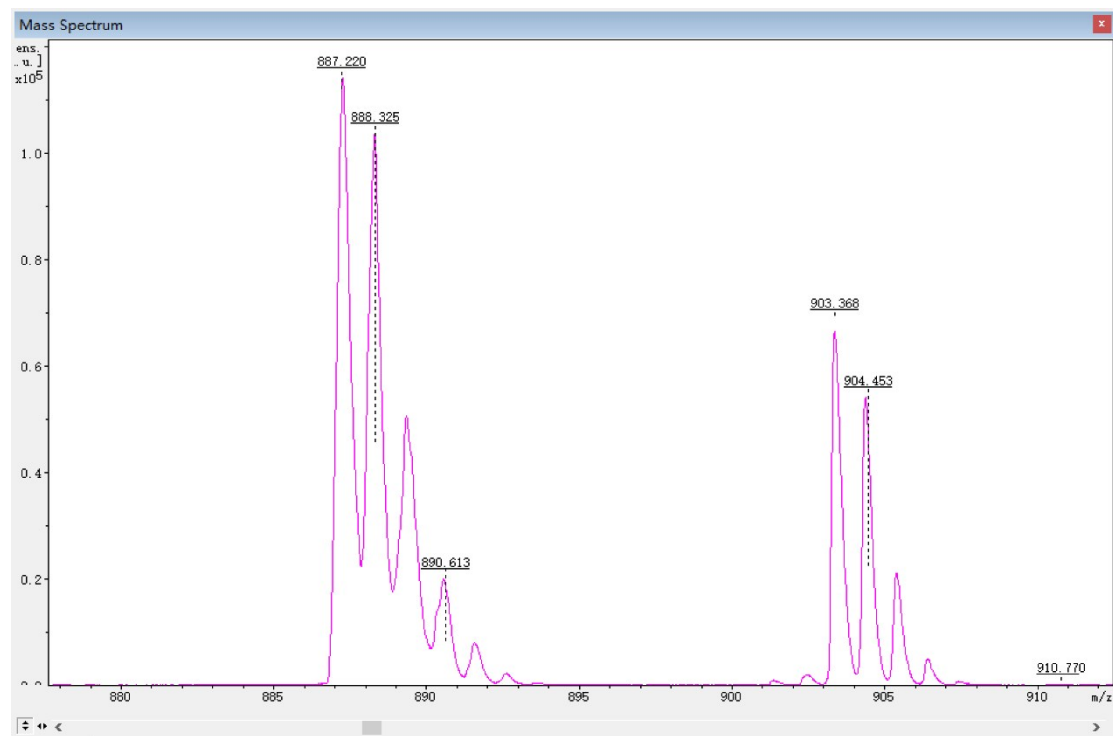


Figure S18. MALDI-TOF MS spectra of 3,6,12-triAC-BPQ.